

Article

High-Intensity Laser-Driven Oxygen Source from CW Laser-Heated Titanium Tape Targets

Kotaro Kondo ^{1,*}, Mamiko Nishiuchi ¹, Hironao Sakaki ¹, Nicholas P. Dover ¹, Hazel F. Lowe ¹, Takumi Miyahara ², Yukinobu Watanabe ², Tim Ziegler ³, Karl Zeil ³, Ulrich Schramm ³, Emma J. Ditter ⁴, George S. Hicks ⁴, Oliver C. Ettliger ⁴, Zulfikar Najmudin ⁴, Hiromitsu Kiriya ¹, Masaki Kando ¹ and Kiminori Kondo ¹

- ¹ Kansai Photon Science Institute (KPSI), National Institutes for Quantum and Radiological Science and Technology (QST), Kizugawa, Kyoto 619-0215, Japan; nishiuchi.mamiko@qst.go.jp (M.N.); sakaki.hironao@qst.go.jp (H.S.); dover.nicholas@qst.go.jp (N.P.D.); hazellowe@gmail.com (H.F.L.); kiryama.hiromitsu@qst.go.jp (H.K.); kando.masaki@qst.go.jp (M.K.); kondo.kiminori@qst.go.jp (K.K.)
- ² Interdisciplinary Graduate School of Engineering Sciences, Kyushu University, Kasuga, Fukuoka 816-8580, Japan; miyahara.t@hitachizosen.co.jp (T.M.); watanabe@aees.kyushu-u.ac.jp (Y.W.)
- ³ Helmholtz-Zentrum Dresden-Rossendorf, Bautzner Landstraße 400, 01328 Dresden, Germany; t.ziegler@hzdr.de (T.Z.); k.zeil@hzdr.de (K.Z.); u.schramm@hzdr.de (U.S.)
- ⁴ John Adams Institute for Accelerator Science, Blackett Laboratory, Imperial College London, London SW7 2AZ, UK; e.ditter15@imperial.ac.uk (E.J.D.); g.hicks11@imperial.ac.uk (G.S.H.); o.ettlinger13@imperial.ac.uk (O.C.E.); z.najmudin@imperial.ac.uk (Z.N.)
- * Correspondence: kondo.kotaro@qst.go.jp; Tel.: +81-774-71-3361

Received: 19 August 2020; Accepted: 16 September 2020; Published: 19 September 2020



Abstract: The interaction of high-intensity laser pulses with solid targets can be used as a highly charged, energetic heavy ion source. Normally, intrinsic contaminants on the target surface suppress the performance of heavy ion acceleration from a high-intensity laser–target interaction, resulting in preferential proton acceleration. Here, we demonstrate that CW laser heating of 5 μm titanium tape targets can remove contaminant hydrocarbons in order to expose a thin oxide layer on the metal surface, ideal for the generation of energetic oxygen beams. This is demonstrated by irradiating the heated targets with a PW class high-power laser at an intensity of $5 \times 10^{21} \text{ W/cm}^2$, showing enhanced acceleration of oxygen ions with a non-thermal-like distribution. Our new scheme using a CW laser-heated Ti tape target is promising for use as a moderate repetition energetic oxygen ion source for future applications.

Keywords: Ti Sapphire laser; high-power laser; laser-driven heavy ion acceleration; surface treatment; CW laser heating; oxygen ion source

1. Introduction

Pettawatt (PW) class high-power lasers can achieve peak focal intensities of over 10^{21} W/cm^2 [1]. The interaction of high-intensity lasers with matter allows us to investigate underlying physics in intense electromagnetic fields [2] and to produce highly energetic ions [3,4], electrons [5,6], electromagnetic radiation such as x-rays [7], and high-energy density states [8]. A promising application of laser-driven heavy ion acceleration is the development of compact particle accelerators made possible by the high accelerating gradient.

For cancer radiotherapy, energetic carbon beams have some advantages over protons since heavier ions have more localized Bragg peaks, which concentrate the damage to the cancer with high biological effect and minimize damage to surrounding healthy tissue [9]. Recently, a multi-ion beam irradiation scheme was proposed [10], enabling us to optimize dose and linear energy transfer (LET) distributions

independently using different nuclides, maximizing the potential of charged particle therapy. Oxygen, which is also mid-Z and has a slightly higher LET than carbon, is a candidate nuclide for such a multi-ion irradiation scheme. In principle, oxygen beams can be generated by the interaction of an intense laser pulse with a gas target, utilizing various acceleration mechanisms suitable for low density plasmas [11–14], although most studies so far have investigated different gas species. However, the optimization of acceleration from gaseous targets is not fully understood, and the generation of stable high flux beams with low divergence and good spatial uniformity as required for applications is still an active subject of research.

On the other hand, so-called Target Normal Sheath Acceleration (TNSA) [15] of ions from the interaction of a high-power laser with a thin-foil solid target has been widely investigated and demonstrated to produce stable beams with low transverse emittance [16], and relatively uniform transverse spatial distribution [17]. In TNSA, fast electrons with typically > MeV energies are efficiently accelerated by the high-intensity laser, and then propagate from the target irradiation side to the rear side of the foil where they generate a strong charge separation, called sheath field. This strong sheath field can then accelerate the ions at the target surface.

However, the strong sheath field only exists at the target surface, which is typically a proton-rich contaminant layer. As protons have the highest charge-to-mass ratio, they are preferentially accelerated. On the other hand, screening by the contaminant plasma reduces the accelerating field for heavy ions coming from the target bulk material producing ions with lower flux and energy. Some techniques have been developed to remove contaminants and enhance heavy ion acceleration, including resistive heating [18,19], ion sputtering [20], pulsed laser desorption [21], laser ablation [22], and detachment of contaminants during the finite rising-edge of the laser pulse [23]. Target irradiation with a CW laser has also been reported to be effective to desorb contaminants and has shown enhancement of heavy ion acceleration using thin targets with 1 μm or less [24–26]. Simple contaminant removal still limits TNSA to materials that can be used to form thin foils, precluding its use to accelerate pure oxygen targets. However, some metals such as titanium form surface oxide layers [27]. If all ion species with a higher charge-to-mass ratio than oxygen are removed, these could be attractive targets for oxygen acceleration using TNSA.

Here, we have investigated the use of Continuous-wave (CW) laser heating to eliminate hydrocarbon contaminants from a 5 μm thick Ti tape, which allows us to operate with a moderate repetition rate such as 10 Hz, leaving a thin stable oxide layer at the surface. We measure the temperature of the CW laser-heated foil, supported by numerical calculation, and use mass spectrometry to demonstrate desorption of hydrocarbons. We then demonstrate the use of the target in a proof-of-principle ion acceleration experiment using a high-intensity laser, showing enhanced oxygen acceleration with a narrow energy range. Our findings are a step forward towards the efficient generation of energetic oxygen beams from a laser-driven ion source in moderate repetition rate.

2. Hydrocarbon Removal by CW Laser Irradiation of Titanium Tape

In order to remove contaminants such as hydrogen, the Ti tape target was heated via irradiation with a compact CW Diode Pumped Solid State Laser (DPSSL) with a 532 nm wavelength (MGL-F-532, CNI, Changchun, China). The CW laser irradiated the Ti tapes with a spot size of ~ 1 mm and power of ~ 1 W in a vacuum chamber with a pressure at below $\sim 10^{-3}$ Pa. The holder is shown in Figure 1a, including the orientation of the CW heating laser with respect to the PW high-power laser. Figure 1b shows an IR thermography image of the CW heated tape, assuming the emissivity of Ti to be 0.5 [28]. The thermal imager (Testo 890, Testo SE & Co. KGaA, Lenzkirch, Germany) provides spatial information and simple installation in the experiment.

The white circle shown in Figure 1b corresponds to a localized region of the Ti tape with a diameter of ~ 4 mm at a temperature above 100 $^{\circ}\text{C}$, indicating that the heated area is limited to a region contained by the tape target holder. The maximum temperature exceeded 1000 $^{\circ}\text{C}$, which is sufficient to desorb hydrogen [29], and is shown by the black point at the center of the white region in Figure 1b.

The exposed thin oxide layer of TiO_2 [30] on the Ti tape target is very stable, with a high melting point in excess of $1800\text{ }^\circ\text{C}$, even higher than that of the bulk Ti.

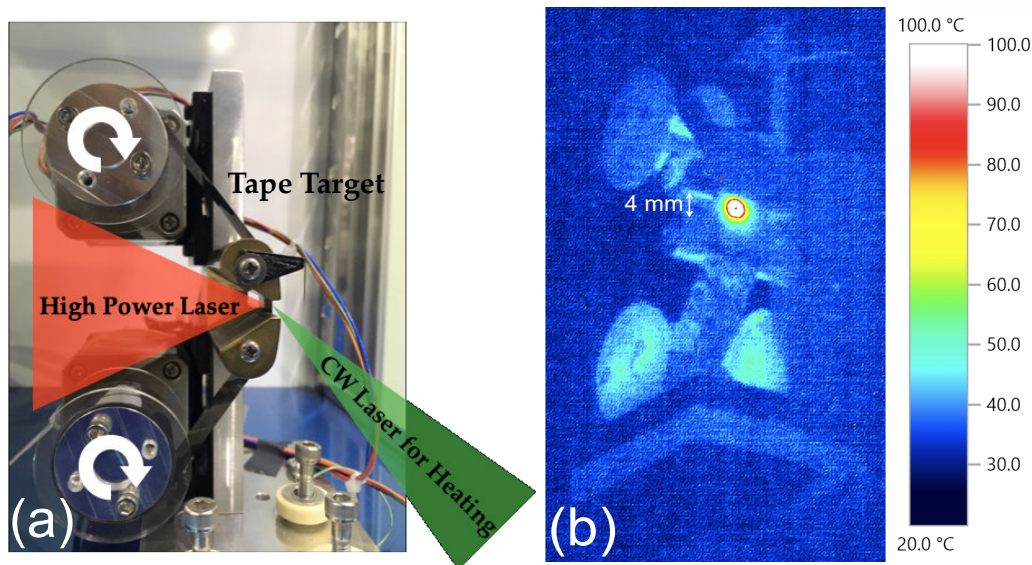


Figure 1. (a) The side view of the tape target overlaid with the orientations of the CW heating laser and the high-power laser for ion acceleration. (b) Temperature distribution of the CW laser-heated tape target, measured by IR thermography. The white region indicates a temperature exceeding $100\text{ }^\circ\text{C}$.

To confirm the measurement, we performed a time-dependent thermal heat transport simulation in polar coordinates with radial symmetric, including thermal conductivity and radiation. In the simulations, the CW laser had a Gaussian profile with four times the standard deviation σ ($D4\sigma$ beam width) of 1 mm, and the absorption of the CW laser to thermal energy in the Ti tape was assumed to be 50% [28]. The simulation assumed that the initial temperature of the system was room temperature (i.e., $24\text{ }^\circ\text{C}$). The simulated temperature as a function of radius is shown in Figure 2 for different times after the start of irradiation. The simulations indicated a localized region several mm in size with a temperature above $100\text{ }^\circ\text{C}$ as well as a smaller region with a temperature beyond $1000\text{ }^\circ\text{C}$, showing good agreement with the IR thermography measurement shown in Figure 1b. The simulation suggests that 100 ms is sufficient to reach more than $1000\text{ }^\circ\text{C}$ over a spatial scale significantly larger than a typical high-power laser focal spot, indicating that the CW laser heating could in principle operate at a rate of up to $\sim 10\text{ Hz}$. Although high-power laser-driven ion acceleration experiments are currently typically performed on a single-shot basis, this technique could be applied to operations up to 10 Hz.

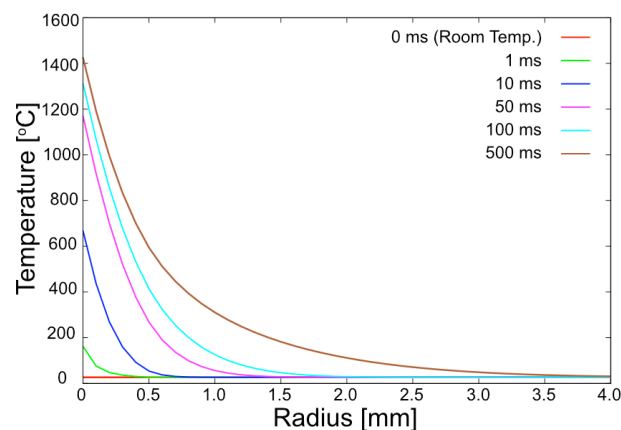


Figure 2. The temperature as a function of radius from the center of the CW laser spot on the tape target, calculated by a time-dependent thermal simulation.

In order to confirm the desorption of the contaminants from the Ti tape by the CW laser heating, we also used a quadrupole mass spectrometer (QMS) as a residual gas analyzer. For this measurement, the CW laser irradiated the Ti tape in vacuum, with CW laser power and spot size of ~ 300 mW and ~ 1 mm, respectively. The measurement results are shown in Figure 3. Emissions of hydrogen, hydroxide and carbon dioxide were observed after the CW laser heating began, providing supporting evidence that the technique can be used to desorb contaminants from the Ti tape.

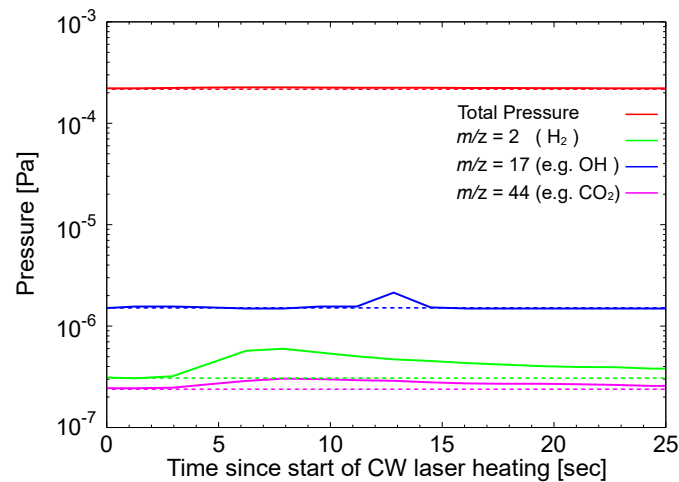


Figure 3. Quadrupole mass spectrometer (QMS) measurement of the partial pressures of different molecular masses as a function of time after the start of laser heating, shown with solid lines. Dashed lines represent the initial pressures before CW laser heating.

3. Demonstration Experiment of Intense Laser-Driven Oxygen Source

The petawatt class J-KAREN-P laser [31,32] at National Institutes for Quantum and Radiological Science and Technology (QST) based on chirped pulse amplification in Ti:Sapphire crystals combined with OPCPA pre-amplifiers operates in the full power mode at a rate of up to 0.1 Hz. It was used on a single shot basis to investigate ion acceleration from the CW laser-heated Ti tape targets described above. In this experiment, the central wavelength of J-KAREN-P is $\lambda_L \sim 810$ nm, with an on-target pulse energy $E_L \sim 10$ J, and pulse length $\tau_L \sim 40$ fs (Full width at half maximum, FWHM). An F/1.4 off-axis parabola (OAP) focused the pulse to a focal spot size $d_L \sim 1.5$ μm (FWHM), resulting in a peak intensity $I_L \sim 5 \times 10^{21}$ W/cm² taking account of the encircled energy, which was used to irradiate Ti tape targets with 5 μm thickness at 45° with *p*-polarization, as shown in Figure 4. A more detailed picture of the tape target system is shown in Figure 1a. The tape is reeled between two rotators with two support bars, providing an accuracy of the target position to within the Rayleigh length of the focused laser, ~ 8 μm . The tape targets were installed in a vacuum chamber with a pressure below $\sim 10^{-3}$ Pa.

When irradiating the Ti tape target without CW laser heating, the high-power laser was unintentionally defocused with respect to the target, resulting in a large spot size and reduced intensity of 1×10^{21} W/cm².

A Thomson Parabola (TP) spectrometer was used to diagnose ions accelerated in the target normal direction. The TP spectrometer employed a 0.42 T magnetic field over 50 mm, combined with an electric field of 25 kV/1.5 cm over 200 mm. A pinhole with 250 μm diameter was placed 430 mm away from the focus position. A micro channel plate (MCP) was installed behind the magnets and the electrodes of the spectrometer to maximize the signal. An electron-multiplying charge-coupled device (EMCCD) with a camera lens imaged the MCP.

The CW DPSSL irradiated the rear side of the target with a spot size of ~ 1 mm and power on target of ~ 1 W for a minimum duration of 10 s before the intense laser irradiation. Then, the intense laser pulse irradiated the tape target while the CW laser was still heating the target, preventing any re-absorption of contaminants, which could have been a serious issue [22].

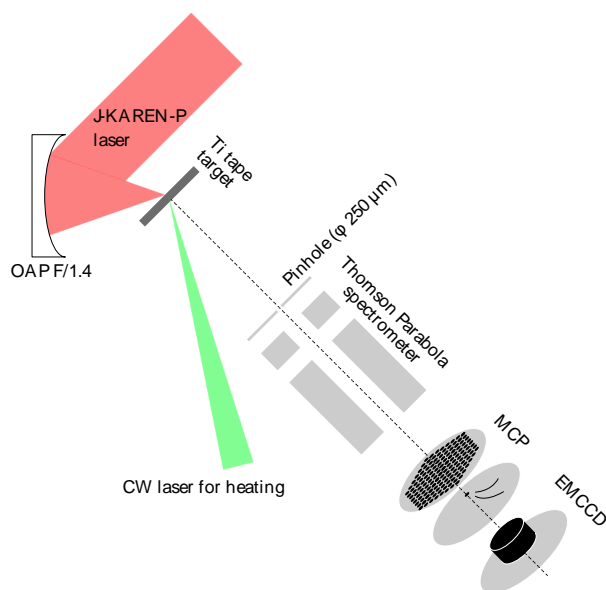


Figure 4. Schematic of the laser-driven ion acceleration experiment with the Ti tape target and Thomson parabola detector.

In order to demonstrate the effect of CW laser heating on laser-driven ion acceleration, images obtained from the TP spectrometer without and with CW laser heating are shown in Figure 5. In Figure 5a, ion tracks corresponding to C^{4+} , C^{5+} , C^{6+} , O^{6+} and protons can clearly be seen over an energy range from the detectable minimum energy, which is determined by the MCP size, to the maximum cut-off energy.

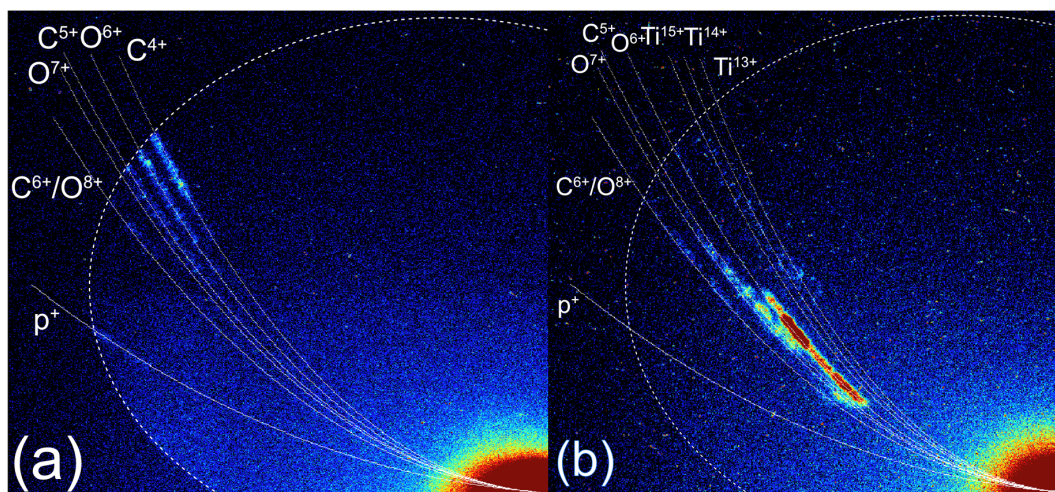


Figure 5. Images of the micro channel plate (MCP) for the Thomson parabola (TP) spectrometer showing parabolic tracks for each ion charge to mass ratios. The brightest points on the bottom right of the images are fixed to the origins of the parabolic curves. The dashed circle shows the MCP size, which determines the minimum detectable energy of ions. (a) shows the ion tracks obtained without CW laser heating, and (b) shows ion tracks obtained with CW laser heating.

The brightest ion track shown in Figure 5b corresponds to O^{6+} , and significantly dimmer lines for C^{5+} , O^{7+} and C^{6+}/O^{8+} were also observed, but no proton signal was visible above the background level. Interestingly, the oxygen lines do not continue to the detectable minimum energy, indicating non-thermal-like ion distribution. Signal consistent with Ti ions is also observed with the CW laser heating. However, the traces of Ti ions are not resolved clearly as the flux was relatively low. Based on

the assumption that ^{48}Ti was the dominant isotope present in the tape target, the Ti charge states were estimated to be Ti^{13+} , Ti^{14+} , and Ti^{15+} , as shown in Figure 5b. The ionization potentials of Ti^{13+} and Ti^{14+} are 787 eV and 864 eV, respectively [33]. These are in a similar range to the ionization potentials of O^{7+} and O^{8+} , which are 739 eV and 871 eV, respectively.

Figure 6 shows the proton and O^{6+} spectra beyond the background level for the case without CW laser heating, calculated from the MCP data in Figure 5a. The proton beam has a typical thermal-like spectrum from the minimum detector cut-off of 11.5 ± 0.3 MeV, to a maximum cut-off of 15.2 ± 0.4 MeV. A just-detectable oxygen beam is observed up to a maximum energy of 2.6 ± 0.1 MeV/u.

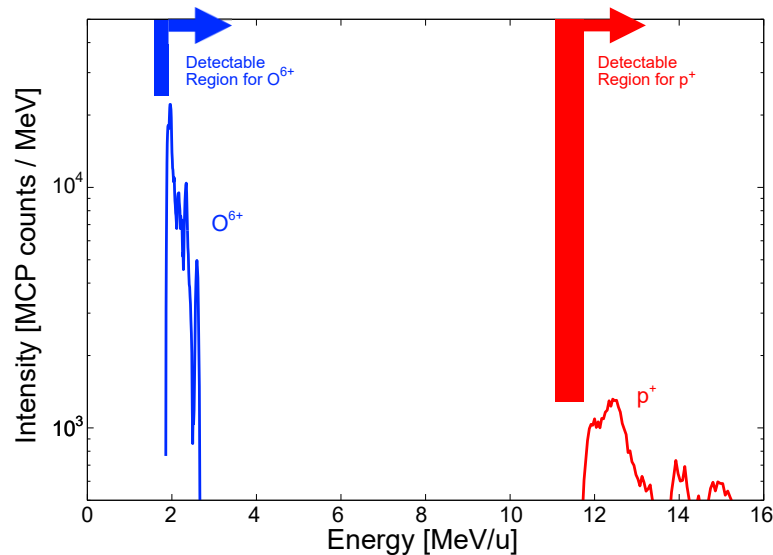


Figure 6. The proton and O^{6+} spectra without CW laser heating. The energy spectrum for both protons and O^{6+} ions extends from the minimum detectable energy to the maximum cut-off energy.

Figure 7 shows Ti^{13+} and O^{6+} spectra beyond the background level for the CW laser-heated target. The Ti^{13+} spectrum shows an energy spread from 1.9 ± 0.1 MeV/u to 2.5 ± 0.1 MeV/u, as shown in Figure 7. On the other hand, the O^{6+} ions appear from 3.3 ± 0.1 MeV/u to 8.3 ± 0.5 MeV/u. The CW laser heating therefore not only increased the flux and energy of the O^{6+} ions, but also generated ions in a relatively narrow energy band ($\Delta E \sim 5$ MeV/u).

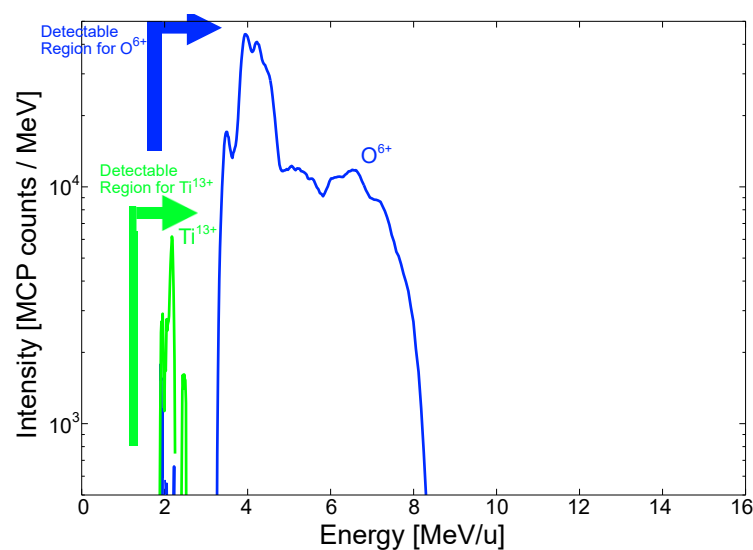


Figure 7. The Ti^{13+} and O^{6+} spectra with CW laser heating. The enhanced acceleration of O^{6+} spectrum shows a non-thermal-like distribution.

4. Discussion

We use a simple analytical approach to discuss the enhanced acceleration of O^{6+} in the case of PW laser irradiation of a CW laser-heated Ti Target. The TP data in Figure 5a shows a clear proton trace in the case without CW laser heating, whereas in Figure 5b it can be seen that the proton trace disappeared when CW laser heating was applied, indicating that CW laser heating removed the hydrogen contaminants, within the sensitivity of the TP detector.

The maximum proton energy observed without CW laser heating can be used for estimating the sheath potential at the rear side because protons have the highest achievable charge-to-mass ratio— Q/A —and are therefore accelerated by the sheath potential more rapidly than other ions with a lower Q/A . For this reason, the maximum proton energy is closely related to the magnitude of the sheath potential. In addition, we assume that the thin contaminant layer does not affect the sheath field potential at the rear side of the target and therefore that the magnitude of the sheath field potential is the same with or without the presence of a contaminant layer.

In the case of the data shown in Figure 5, unfortunately the laser intensity on target was 20% of the typical intensity during this experiment, giving rise to a lower-than-expected maximum proton energy of 15.2 ± 0.4 MeV from PW laser irradiation of the Ti target without CW laser heating. For a typical laser intensity (I_L) of 5×10^{21} W/cm², the maximum proton energy (E_p) can be estimated using the spot-size scaling [34] $E_p \propto I_L^{1/4}$, which gives $E_p \sim 20$ MeV. This calculation is supported by a previous result where a 5 μ m steel tape target was irradiated at 5×10^{21} W/cm² without CW laser heating, under laser conditions comparable to the experiment presented here, and the measured maximum proton energy was in excess of 20 MeV [34]. Therefore, it is reasonable to assume that PW laser irradiation at 5×10^{21} W/cm² of the Ti target without CW laser heating would generate a maximum proton energy in the region of ~ 20 MeV, corresponding to a sheath potential of ~ 20 MV.

The spectrum in Figure 6 shows that the $^{16}O^{6+}$ ions occupy a narrow energy band with a maximum measured energy, $E_{O^{6+}}$, of 8.3 ± 0.5 MeV/u. Analytically, the corresponding potential, $\Phi_{O^{6+}}$, required to accelerate O^{6+} to the energy, $E_{O^{6+}}$, is given by

$$\Phi_{O^{6+}} \text{ [MV]} = \frac{E_{O^{6+}} \text{ [MeV/u]}}{e(Q/A)} \sim 22.1 \pm 1.3 \text{ [MV]} \quad (1)$$

where e is the elementary charge and Q/A is the charge to mass ratio of ions. The calculated value $\Phi_{O^{6+}} = 22.1 \pm 1.3$ MV agrees with the value of sheath potential of ~ 20 MV estimated above using the scaling of maximum proton energy with laser spot-size scaling. This indicates that, as in the case of protons, the O^{6+} ions are accelerated by the sheath potential without any shielding.

Figure 5 shows that Ti ions were only detected when CW laser heating was applied, indicating that removal of contaminants by CW laser heating has a significant effect on the ion acceleration dynamics in the sheath field. The Ti ions are shielded by the O^{6+} – O^{8+} ions, which have a higher Q/A and are accelerated more efficiently by the sheath field. In order to confirm this mechanism, we again apply Equation (1) to consider the potential required to achieve the minimum value of $E_{O^{6+}} = 3.3 \pm 0.1$ MeV/u, which is $\Phi_{O^{6+}} = 8.8 \pm 0.3$ MV. In the case of $^{48}Ti^{13+}$, Figure 7 shows a maximum measured energy of 2.5 ± 0.1 MeV/u that corresponds to $\Phi_{Ti^{13+}} = 9.2 \pm 0.4$ MV. Therefore, we can conclude that in the thin titanium oxide layer exposed by the CW laser heating, Ti ions with a lower Q/A are accelerated successively after the oxygen ions with higher Q/A .

The sheath potentials from experimental results with CW laser heating and of proton acceleration from contaminants without heating are shown in Table 1. Although further investigation including a particle-in-cell simulation is required to understand the mechanism of the narrow energy band spectrum [19,35–38], the demonstration with the CW laser-heated Ti tape shows the enhancement of the oxygen ion beams and the suppression of ions from hydrocarbon contaminants. The proposed concept for oxygen ion acceleration could apply to not only titanium but also to metals with thin oxide

layers such as aluminum [39] and stainless steel [40]. Moreover, silicon nitride tapes [41] could be used for moderate-repetition laser-driven nitrogen ion sources as well.

Table 1. Accelerated kinetic energies and the corresponding potentials Φ for typical ion species with the CW laser heating. The energy and potential for proton without the heating are estimated using the spot-size scaling [34].

Ion Species	Q/A	Kinetic Energy [MeV/u]	Φ [MV]
H ⁺ w/o heating	1/1	~20 (Max)	~20
O ⁶⁺ w heating	6/16	8.3 ± 0.5 (Max)	22.1 ± 1.3
O ⁶⁺ w heating	6/16	3.3 ± 0.1 (Min.)	8.8 ± 0.3
Ti ¹³⁺ w heating	13/48	2.5 ± 0.1 (Max)	9.2 ± 0.4

5. Conclusions

In this paper, we have shown the development of a target suitable for efficient oxygen acceleration from high-intensity laser irradiation. We show that by applying CW laser heating to a thick Ti target, it is possible to heat the target sufficiently to desorb hydrocarbon contaminants, leaving only an oxide surface layer. A proof-of-principle experiment using a high-intensity laser to irradiate the target was performed, demonstrating significantly suppressed acceleration of protons and preferential acceleration of oxygen ions when the CW laser heating was applied. A simple analysis of experimental data indicates that the thin, stable native oxide layer on the surface of the Ti tape target is exposed by the CW laser heating, allowing the oxygen ions to be accelerated by the sheath field without shielding from the lighter contaminant ions. This demonstrates that, with further development, the proposed method of CW laser heating of a Ti tape target could be promising as a moderate repetition of ~10 Hz, high-energy oxygen ion sources for future applications, such as multi-ion irradiation radiotherapy [10].

Author Contributions: Conceptualization, K.K. (Kotaro Kondo), M.N., H.S. and N.P.D.; Methodology, K.K. (Kotaro Kondo); Software, K.K. (Kotaro Kondo), H.S. and N.P.D.; validation, K.K. (Kotaro Kondo), M.N., H.S., N.P.D. and H.F.L.; investigation, K.K. (Kotaro Kondo), M.N., H.S., N.P.D., H.F.L., T.M., Y.W., T.Z., K.Z., U.S., E.J.D., G.S.H., O.C.E. and Z.N.; writing—original draft preparation, K.K. (Kotaro Kondo); writing—review and editing, K.K. (Kotaro Kondo), M.N., H.S., N.P.D., H.F.L., G.S.H., O.C.E. and H.K.; supervision, M.K.; project administration, K.K. (Kiminori Kondo). All authors have read and agreed to the published version of the manuscript.

Funding: Japan Society for the Promotion of Science Grant Number JP 16K17686 and 16K05506, Japan; JST-MIRAI R & D Programm Grant Number JPMJ17A1, Japan; JST PRESTO Grant Number JPMJPR16P9, Japan; QST International Research Initiative (AAA98) and Creative Research (ABACS), Japan; Mitsubishi Foundation (ID:28131), Japan.

Acknowledgments: The authors acknowledge contributions by the Kansai Photon Science Institute staff at the National Institutes for Quantum and Radiological Science, and Yuji Fukuda, Yasuhiro Miyasaka, Nobuhiko Nakanii, Koichi Ogura, Alexander S. Pirozhkov, and Akito Sagisaka.

Conflicts of Interest: The authors declare no conflict of interest.

References

- Danson, C.N.; Haefner, C.; Bromage, J.; Butcher, T.; Chanteloup, J.-C.F.; Chowdhury, E.A.; Galvanauskas, A.; Gizzi, L.A.; Hein, J.; Hillier, D.I.; et al. Petawatt and exawatt class lasers worldwide. *High-Power Laser Sci. Eng.* **2019**, *7*, e54. [[CrossRef](#)]
- Di Piazza, A.; Müller, C.; Hatsagortsyan, K.Z.; Keitel, C.H. Extremely high-intensity laser interactions with fundamental quantum systems. *Rev. Mod. Phys.* **2012**, *84*, 1177. [[CrossRef](#)]
- Macchi, A.; Borghesi, M.; Passoni, M. Ion acceleration by super intense laser-plasma interaction. *Rev. Mod. Phys.* **2013**, *85*, 751. [[CrossRef](#)]
- Daido, H.; Nishiuchi, M.; Pirozhkov, A.S. Review of laser-driven ion sources and their applications. *Rep. Prog. Phys.* **2012**, *75*, 056401. [[CrossRef](#)] [[PubMed](#)]
- Malka, V.; Faure, J.; Gauduel, Y.A.; Lefebvre, E.; Rousse, A.; Phuoc, K.T. Principles and applications of compact laser-plasma accelerators. *Nat. Phys.* **2008**, *4*, 447. [[CrossRef](#)]

6. Esarey, E.; Schroeder, C.B.; Leemans, W.P. Physics of laser-driven plasma-based electron accelerators. *Rev. Mod. Phys.* **2009**, *81*, 1229. [[CrossRef](#)]
7. Pirozhkov, A.S.; Esirkepov, T.Z.; Pikuz, T.A.; Faenov, A.Y.; Ogura, K.; Hayashi, Y.; Kotaki, H.; Ragozin, E.N.; Neely, D.; Kiriya, H.; et al. Burst intensification by singularity emitting radiation in multi-stream flows. *Sci. Rep.* **2017**, *7*, 17968. [[CrossRef](#)]
8. Soloviev, A.; Burdonov, K.; Chen, S.N.; Ereemeev, A.; Korzhimanov, A.; Pokrovskiy, G.V.; Pikuz, T.A.; Revet, G.; Sladkov, A.; Ginzburg, V.; et al. Experimental evidence for short-pulse laser heating of solid-density target to high bulk temperatures. *Sci. Rep.* **2017**, *7*, 12144. [[CrossRef](#)]
9. Mohamad, O.; Sishc, B.J.; Saha, J.; Pompos, A.; Rahimi, A.; Story, M.D.; Davis, A.J.; Kim, D.W.N. Carbon Ion Radiotherapy: A Review of Clinical Experiences and Preclinical Research, with an Emphasis on DNA Damage/Repair. *Cancer* **2017**, *9*, 66. [[CrossRef](#)]
10. Inaniwa, T.; Kanematsu, N.; Noda, K.; Kamada, T. Treatment planning of intensity modulated composite particle therapy with dose and linear energy transfer optimization. *Phys. Med. Biol.* **2017**, *62*, 5180. [[CrossRef](#)]
11. Willingale, L.; Mangles, S.P.D.; Nilson, P.M.; Clarke, R.J.; Dangor, A.E.; Kaluza, M.C.; Karsch, S.; Lancaster, K.L.; Mori, W.B.; Najmudin, Z.; et al. Collimated Multi-MeV Ion Beams from High-Intensity Laser Interactions with Underdense Plasma. *Phys. Rev. Lett.* **2006**, *96*, 245002. [[CrossRef](#)] [[PubMed](#)]
12. Palmer, C.A.J.; Dover, N.P.; Pogorelsky, I.; Babzien, M.; Dudnikova, G.I.; Ispiryan, M.; Polyanskiy, M.N.; Schreiber, J.; Shkolnikov, P.; Yakimenko, V.; et al. Monoenergetic Proton Beams Accelerated by a Radiation Pressure Driven Shock. *Phys. Rev. Lett.* **2011**, *106*, 014801. [[CrossRef](#)] [[PubMed](#)]
13. Chen, S.N.; Vranic, M.; Gangolf, T.; Boella, E.; Antici, P.; Bailly-Grandvaux, M.; Loiseau, P.; Pépin, H.; Revet, G.; Santos, J.J.; et al. Collimated protons accelerated from an overdense gas jet irradiated by a 1 μ m wavelength high-intensity short-pulse laser. *Sci. Rep.* **2017**, *7*, 13505. [[CrossRef](#)] [[PubMed](#)]
14. Krushelnick, K.; Clark, E.L.; Najmudin, Z.; Salvati, M.; Santala, M.I.K.; Tatarakis, M.; Dangor, A.E.; Malka, V.; Neely, D.; Allott, R.; et al. Multi-MeV Ion Production from High-Intensity Laser Interactions with Underdense Plasmas. *Phys. Rev. Lett.* **1999**, *83*, 737. [[CrossRef](#)]
15. Wilks, S.C.; Langdon, A.B.; Cowan, T.E.; Roth, M.; Singh, M.; Hatchett, S.; Key, M.H.; Pennington, D.; MacKinnon, A.; Snavely, R.A. Energetic proton generation in ultra-intense laser–solid interactions. *Phys. Plasmas* **2001**, *8*, 542. [[CrossRef](#)]
16. Cowan, T.E.; Fuchs, J.; Ruhl, H.; Kemp, A.; Audebert, P.; Roth, M.; Stephens, R.; Barton, I.; Blazevic, A.; Brambrink, E.; et al. Ultralow Emittance, Multi-MeV Proton Beams from a Laser Virtual-Cathode Plasma Accelerator. *Phys. Rev. Lett.* **2004**, *92*, 204801. [[CrossRef](#)]
17. Fuchs, J.; Cowan, T.E.; Audebert, P.; Ruhl, H.; Gremillet, L.; Kemp, A.; Allen, M.; Blazevic, A.; Gauthier, J.-C.; Geissel, M.; et al. Spatial Uniformity of Laser-Accelerated Ultrahigh-Current MeV Electron Propagation in Metals and Insulators. *Phys. Rev. Lett.* **2003**, *91*, 255002. [[CrossRef](#)]
18. Hegelich, M.; Karsch, S.; Pretzler, G.; Habs, D.; Witte, K.; Guenther, W.; Allen, M.; Blazevic, A.; Fuchs, J.; Gauthier, J.C.; et al. MeV Ion Jets from Short-Pulse-Laser Interaction with Thin Foils. *Phys. Rev. Lett.* **2002**, *89*, 085002. [[CrossRef](#)]
19. Hegelich, B.M.; Albright, B.J.; Cobble, J.; Flippo, K.; Letzring, S.; Paffett, M.; Ruhl, H.; Schreiber, J.; Schulze, R.K.; Fernández, J.C. Laser acceleration of quasi-monoenergetic MeV ion beams. *Nature* **2006**, *439*, 441. [[CrossRef](#)]
20. Allen, M.; Patel, P.K.; Mackinnon, A.; Price, D.; Wilks, S.; Morse, E. Direct Experimental Evidence of Back-Surface Ion Acceleration from Laser-Irradiated Gold Foils. *Phys. Rev. Lett.* **2004**, *93*, 265004. [[CrossRef](#)]
21. Hoffmeister, G.; Bellei, C.; Harres, K.; Ivanov, D.; Kraus, D.; Pelka, A.; Rethfeld, B.; Schaumann, G.; Roth, M. Influence of fs-laser desorption on target normal sheath accelerated ions. *Phys. Rev. Accel. Beams* **2013**, *16*, 041304. [[CrossRef](#)]
22. Sommer, P.; Metzkes-Ng, J.; Brack, F.-E.; Cowan, T.E.; Kraft, S.D.; Obst, L.; Rehwald, M.; Schlenvoigt, H.-P.; Schramm, U.; Zeil, K. Laser-ablation-based ion source characterization and manipulation for laser-driven ion acceleration. *Plasma Phys. Control. Fusion* **2018**, *60*, 054002. [[CrossRef](#)]
23. Nishiuchi, M.; Dover, N.P.; Hata, M.; Sakaki, H.; Kondo, K.; Lowe, H.F.; Miyahara, T.; Kiriya, H.; Koga, J.K.; Iwata, N.; et al. Dynamics of laser-driven heavy-ion acceleration clarified by ion charge states. *Phys. Rev. Res.* **2020**, *2*, 033081. [[CrossRef](#)]

24. Jung, D.; Yin, L.; Gautier, D.C.; Wu, H.-C.; Letzring, S.; Dromey, B.; Shah, R.; Palaniyappan, S.; Shimada, T.; Johnson, R.P.; et al. Laser-driven 1 GeV carbon ions from preheated diamond targets in the break-out afterburner regime. *Phys. Plasmas* **2013**, *20*, 083103. [[CrossRef](#)]
25. Safronov, K.V.; Gorokhov, S.A.; Flegentov, V.A.; Potapov, A.V.; Gavrilov, D.S.; Kakshin, A.G.; Loboda, E.A.; Vikhlyaev, D.A. Laser-driven ion acceleration from thin foils heated by CW laser. *Phys. Plasmas* **2018**, *25*, 103114. [[CrossRef](#)]
26. Lindner, F.H.; McCary, E.; Jiao, X.; Ostermayr, T.M.; Roycroft, R.; Tiwari, G.; Hegelich, B.M.; Schreiber, J.; Thirolf, P.G. En-route to the fission–fusion reaction mechanism: A status update on laser-driven heavy ion acceleration. *Plasma Phys. Control. Fusion* **2019**, *61*, 055002. [[CrossRef](#)]
27. Wang, G.; Li, J.; Lv, K.; Zhang, W.; Ding, X.; Yang, G.; Liu, X.; Jiang, X. Surface thermal oxidation on titanium implants to enhance osteogenic activity and *in vivo* osseointegration. *Sci. Rep.* **2016**, *6*, 31769. [[CrossRef](#)]
28. Bradshaw, F.J. The optical emissivity of Titanium and Zirconium. *Proc. Phys. Soc. B* **1950**, *63*, 573. [[CrossRef](#)]
29. Tsuchiya, B.; Nagata, S.; Ohtsu, N.; Toh, K.; Shikama, T. Thermal desorption of hydrogen at the Titanium hydride-oxide interface. *Mater. Trans.* **2005**, *46*, 196. [[CrossRef](#)]
30. Koch, D.; Manzhos, S. On the Charge State of Titanium in Titanium Dioxide. *J. Phys. Chem. Lett.* **2017**, *8*, 1593. [[CrossRef](#)]
31. Kiriya, H.; Pirozhkov, A.S.; Nishiuchi, M.; Fukuda, Y.; Ogura, K.; Sagisaka, A.; Miyasaka, Y.; Mori, M.; Sakaki, H.; Dover, N.P.; et al. High-contrast high-intensity repetitive petawatt laser. *Opt. Lett.* **2018**, *43*, 2595. [[CrossRef](#)] [[PubMed](#)]
32. Pirozhkov, A.S.; Fukuda, Y.; Nishiuchi, M.; Kiriya, H.; Sagisaka, A.; Ogura, K.; Mori, M.; Kishimoto, M.; Sakaki, H.; Dover, N.P.; et al. Approaching the diffraction-limited, bandwidth-limited Petawatt. *Opt. Express* **2017**, *25*, 20486–20501. [[CrossRef](#)] [[PubMed](#)]
33. NIST Atomic Spectra Database Ionization Energies Form. Available online: <https://physics.nist.gov/PhysRefData/ASD/ionEnergy.html> (accessed on 1 September 2020).
34. Dover, N.P.; Nishiuchi, M.; Sakaki, H.; Kondo, K.; Alkhimova, M.A.; Faenov, A.Y.; Hata, M.; Iwata, N.; Kiriya, H.; Koga, J.K.; et al. Effect of small focus on electron heating and proton acceleration in ultrarelativistic laser-solid interactions. *Phys. Rev. Lett.* **2020**, *124*, 084802. [[CrossRef](#)] [[PubMed](#)]
35. Allen, M.; Sentoku, Y.; Audebert, P.; Blazevic, A.; Cowan, T.; Fuchs, J.; Gauthier, J.C.; Geissel, M.; Hegelich, M.; Karsch, S.; et al. Proton spectra from ultraintense laser–plasma interaction with thin foils: Experiments, theory, and simulation. *Phys. Plasmas* **2003**, *10*, 3283. [[CrossRef](#)]
36. Bychenkov, V.Y.; Novikov, V.N.; Batani, D.; Tikhonchuk, V.T.; Bochkarev, S.G. Ion acceleration in expanding multispecies plasmas. *Phys. Plasmas* **2004**, *11*, 3242. [[CrossRef](#)]
37. Dollar, F.; Matsuoka, T.; Petrov, G.M.; Thomas, A.G.R.; Bulanov, S.S.; Chvykov, V.; Davis, J.; Kalinchenko, G.; McGuffey, C.; Willingale, L.; et al. Control of Energy Spread and Dark Current in Proton and Ion Beams Generated in High-Contrast Laser Solid Interactions. *Phys. Rev. Lett.* **2011**, *107*, 065003. [[CrossRef](#)]
38. Dover, N.P.; Palmer, C.A.J.; Streeter, M.J.V.; Ahmed, H.; Albertazzi, B.; Borghesi, M.; Carroll, D.C.; Fuchs, J.; Heathcote, R.; Hilz, P.; et al. Buffered high charge spectrally-peaked proton beams in the relativistic-transparency regime. *New J. Phys.* **2016**, *18*, 013038. [[CrossRef](#)]
39. Evertson, J.; Bertrama, F.; Zhang, F.; Rullika, L.; Merte, L.R.; Shipilina, M.; Soldemoe, M.; Ahmadi, S.; Vinogradov, N.; Carlad, F.; et al. The thickness of native oxides on aluminum alloys and single crystals. *Appl. Surf. Sci.* **2015**, *349*, 826. [[CrossRef](#)]
40. Olsson, C.-O.A.; Landolt, D. Passive films on stainless steels—chemistry, structure and growth. *Electrochim. Acta* **2003**, *48*, 1093. [[CrossRef](#)]
41. Ma, S.; Ning, X.; Fu, T.; Zhou, H.; Chen, K. Fabrication of Thick Silicon Nitride Substrate by Tape Casting. *Key Eng. Mater.* **2008**, *368*, 875. [[CrossRef](#)]

